Research Square

Preprints are preliminary reports that have not undergone peer review.
They should not be considered conclusive, used to inform clinical practice,
or referenced by the media as validated information.

A novel biological parcellation of anterior cingulate cortex as identified by a functional reversal point in error monitoring

Camila Dias
University of Coimbra
Teresa Sousa
University of Coimbra
Assunta Ciarlo
Maastricht University
Michael Lührs
Maastricht University
Rainer Goebel
Maastricht University
Miguel Castelo-Branco
mcbranco@fmed.uc.pt

University of Coimbra

Research Article

Keywords: Anterior cingulate cortex (ACC), functional subregions, error monitoring, 7T fMRI

Posted Date: October 20th, 2026

DOI: https://doi.org/10.21203/rs.3.rs-11249829/v1

License: This work is licensed under a Creative Commons Attribution 4.0 International License.
Read Full License

Additional Declarations: No competing interests reported.

Abstract

The anterior cingulate cortex (ACC) plays a key role in error monitoring, signalling the need for cognitive control to optimize performance. Although this region comprises multiple subregions, their precise functional organization and contributions to error monitoring remain unclear. We investigated ACC functional parcellation during error monitoring using 7T functional magnetic resonance imaging (fMRI). Ten participants performed three variations of a fast-response task: one focused on error commission (without feedback), another on feedback processing, and the last on error observation. We found that distinct ACC subregions were differentially engaged during these processes. Specifically, we identified a polarity reversal in ACC responses to self-generated errors versus correct instances. This reversal separated dorsal subregions — more responsive to errors — from rostroventral subregions — more active during correct outcomes. In contrast, only rostroventral regions differentiated correct from erroneous responses in the observation condition. These findings provide insight into the functional organization of the ACC, suggesting a distinction between dorsal subregions, primarily involved in cognitive aspects of error monitoring, and rostroventral subregions, that may support socioemotional aspects of error processing.

1. Introduction

The anterior cingulate cortex (ACC) is a brain region that surrounds the genu of the corpus callosum, which plays important roles in a variety of domains ranging from cognitive control to emotional processing (Sakata et al. 2019). Due to its diverse functions, the ACC has been divided into dorsal (dACC), pregenual/rostral (pgACC), and subgenual/ventral ACC (sgACC) (Sakata et al. 2019; Tang et al. 2019; Zhou et al. 2024). The dACC has also been termed anterior midcingulate cortex (Vogt 2016) and rostral cingulate zone (Picard and Strick 1996). Hereafter, we use the most common term in the error monitoring literature — dACC.

Previous neuroimaging studies have suggested that the dACC is particularly implicated in cognitive processing and the pgACC/sgACC in affective processing (Bush et al. 2000; Yu et al. 2011; Vogt 2016) and autonomic regulation (Fu et al. 2023). While the sgACC seems to play an important role in regulating emotions (Beckmann et al. 2009; Silk et al. 2022) and autonomic control (Stevens et al. 2011), the pgACC has been linked to reward processing (Beckmann et al. 2009) and the integration of affective, cognitive, and autonomic signals (Stevens et al. 2011; Silk et al. 2022). The dACC has been linked to a broad range of executive functions, including the monitoring of errors and conflict, as well as the mediation of post-error adjustments (Heilbronner and Hayden 2016; Ullsperger 2017). It has been proposed that the dACC monitors external and internal conditions, evaluates actions by comparing predicted to observed outcomes, and provides information to downstream circuits to update predictions and optimize future behaviour (Shane et al. 2008; Heilbronner and Hayden 2016; Dixon et al. 2017).

When errors occur, the dACC tracks them and signals the need for additional control and cognitive resources (Heilbronner and Hayden 2016; Weiss et al. 2018). It has been suggested that error-related

activity may shift from dorsal to rostroventral areas of the ACC as the emotional context of error processing intensifies. While the dACC appears primarily responsible for the cognitive aspects of error monitoring, the pgACC and sgACC may be more involved in emotional and motivational aspects (Shane et al. 2008; Marinkovic and Rosen 2022). Although specialisations of ACC subregions for specific error monitoring functions have been repeatedly suggested (Jahn et al. 2014; Kolling et al. 2016; Shenhav et al. 2018; Weiss et al. 2018), the functional dissociation of these subregions remains to be clarified (Ullsperger 2017; Smith et al. 2021).

The neural correlates of error monitoring have been extensively studied using electroencephalography (EEG) (Chavarriaga et al. 2014; Bhattacharyya et al. 2017), largely because of its temporal resolution (Boly et al. 2016). EEG studies have identified distinct error signals associated with different processes. The error-related negativity (ERN) is a midfrontal negative event-related potential (ERP) that emerges after the execution of an erroneous action (Chavarriaga et al. 2014; Bhattacharyya et al. 2017). In contrast, the feedback-related negativity (FRN) occurs after receiving external feedback indicating an incorrect action (Chavarriaga et al. 2014; Fidêncio et al. 2022). Additionally, when a person recognizes an error made by another individual, an observation ERN (oERN) is elicited (Bhattacharyya et al. 2017; Fidêncio et al. 2022). The dACC has been identified as the neural source of all these ERPs (Gruendler et al. 2011; Ullsperger et al. 2014), and a considerable overlap between these components has been suggested (Gruendler et al. 2011). However, due to EEG's low spatial resolution (Boly et al. 2016), functional magnetic resonance imaging (fMRI) is a more suitable technique for examining the spatial dissociation of distinct error monitoring processes.

Using fMRI, Holroyd et al. (2004) suggested that error commission and error feedback activate the same region of the dACC. Furthermore, Shane et al. (2008) provided evidence for common neural circuitry underlying the execution and observation of errors, including the dACC and pgACC. In contrast, Apps & Ramnani (2014) and Lockwood et al. (2018) suggested a functional dissociation within the ACC between the execution and observation of errors. However, to date, no fMRI study has directly compared ACC activity following error commission, error feedback, and error observation.

This study explored the functional parcellation of the ACC during error monitoring using 7T fMRI. Participants performed three variations of a fast-response task: one targeting error commission, another focusing on feedback processing, and the third on error observation. In the first variation, participants responded without receiving feedback; in the second, performance feedback was provided; and in the third, participants observed responses provided by the computer. Because these processes differ in the source and type of error information — internally generated response errors, externally signalled errors through feedback, and errors generated by another agent and observed by the participant — we hypothesized that error commission, error feedback, and error observation recruit spatially dissociable ACC subregions.

Given the ACC's role in autonomic regulation (Beissner et al. 2013; Seamans and Floresco 2022) and the fact that errors often lead to changes in skin conductance (Hajcak et al. 2003; Holper et al. 2013), we

also examined the relationship between ACC activity and electrodermal activity (EDA) to determine which subregions are involved in autonomic responses to errors. Thus, a secondary research question was which ACC subregion, the sgACC or pgACC, plays a predominant role in autonomic regulation during error monitoring. While both regions contribute to autonomic regulation, their specific functions in this context remain unclear (Vogt 2005).

2. Methods

2.1. Participants

Ten neurotypical volunteers (five females, mean age 25.70 ± 4.50 years) participated in this study. Individuals with neurological or psychiatric disorders were not included, and all participants had normal or corrected-to-normal visual acuity. All volunteers were right-handed, as evaluated by the mean laterality index (Oldfield 1971), which was 92.50 ± 11.37. Every participant completed the magnetic resonance imaging (MRI) safety questionnaire and provided written informed consent in accordance with the Declaration of Helsinki prior to participation. The study followed the safety guidelines for research on humans and was approved by the Ethics Review Committee of the Faculty of Psychology and Neuroscience of Maastricht University (approval reference: OZL_253_75_05_2022). Participants were enrolled in bachelor's, master's, or doctoral programs, internships, or exchange programs at Maastricht University. Bachelor’s and master’s students were eligible to earn study credits for their participation. All analyses included the full sample of participants.

To ensure proper executive functioning, participants completed the Eriksen flanker task outside the scanner. The task was implemented using pyFlies (Dejanović et al. 2021) and consisted of 80 trials. Mean accuracy was 97.62 ± 2.32%, revealing normal executive functioning and strong ability to perform fast-response tasks. Mean reaction times were 418.94 ± 33.51 ms for congruent and 489.08 ± 39.61 ms for incongruent trials. As expected, reaction times were longer for incongruent trials (Mann-Whitney U test, $Z = 2.80$, $p = 0.005$), consistent with the typical flanker effect.

2.2. Task

To study the functional parcellation of the ACC, we adapted a fast-response task from our previous studies (Estiveira et al. 2022; Dias et al. 2024, 2025). This task required participants to integrate emotional facial expressions and gaze cues before making a keypress-based response and was designed to elicit a high error rate. The updated version included three conditions (one of the three conditions was assigned to each run): the *response* condition, where participants responded without receiving feedback; the *feedback* condition, where performance feedback was provided; and the *observation* condition, where participants evaluated responses provided by the computer. There were four possible responses (left-click using the left hand, right-click using the left hand, left-lick using the right hand, and right-click using the right hand) and correct responses depended on the interpretation of four cues (emotional expression, gaze direction, frame shape, and frame colour) and additional information provided at the beginning and middle of each run.

To press the correct button (Fig. 1a), participants needed to integrate the emotional expression, gaze direction, and frame colour cues. If the frame was green, a happy face indicated to click in the direction of the face's eye gaze, and a sad face indicated to click in the opposite direction of the face's eye gaze; if the frame was red, the instructions were reversed (a happy face indicated to click in the opposite direction of the face's eye gaze, and a sad face indicated to click in the direction of the face's eye gaze).

To choose the correct hand, participants had to integrate the frame colour and shape cues with the information given in one of the schematics with a black background provided in Fig. 1b. One schematic was presented at the beginning of each run, and the other was introduced midway (after 24 trials), reversing the response rules. According to the first schematic (Fig. 1b, left panel), a green rectangle or red diamond indicated a right-hand response, while a red rectangle or green diamond indicated a left-hand response.

At the beginning of each run, participants were informed about the condition they would perform (response, feedback, or observation). Participants completed six experimental runs (two of each condition), with 48 trials per run. The order of the runs was pseudo-randomized to ensure that all conditions were conducted within the first three runs, helping to account for learning effects. One participant completed only five runs due to tiredness, missing the second observation run.

In the response and observation runs, the experimental paradigm consisted of five periods (Fig. 2). Each trial included an instruction, an action period, and three gaps. The gap periods displayed a black background with a white fixation cross at the centre of the screen, serving as inter-stimulus intervals to minimize overlap in the blood oxygenation level-dependent (BOLD) responses evoked by successive events. The first gap, lasting 500 ms, occurred before the instruction phase. The instruction was then presented for 500 ms, with the order randomized across cues, with all of them counterbalanced (happy and sad faces, green and red frames, rectangle and diamond frames, and left and right gaze directions). Following the instruction, a variable-duration gap period (1000 ms, 2000 ms, or 3000 ms) preceded the action phase, which lasted 1000 ms. Finally, a third gap period of variable duration (1000 ms, 2000 ms, or 3000 ms) followed the action phase. The action phase differed between the response and observation conditions. In the response condition runs, the action period consisted of a black background during which participants should press the chosen button. In the observation condition, one of four possible responses — left-click with the left hand, right-click with the left hand, left-click with the right hand, or right-click with the right hand — was displayed. These responses could be correct (probability = 2/3) or incorrect (probability = 1/3), but participants were not aware of the probabilities. Additionally, observation condition runs included eight randomly distributed catch trials, each lasting 3000 ms. During these trials, participants were required to indicate whether the previous trial was correct or incorrect to ensure they remained attentive. Each run of the response and observation conditions lasted approximately 6 minutes.

The feedback condition (Fig. 2) was similar to the response condition but included an additional feedback period and a fourth gap period. At the end of the third gap period (which, in this condition,

lasted 1500 ms, 2500 ms, or 3500 ms instead of 1000 ms, 2000 ms, or 3000 ms), performance feedback was provided for 500 ms, which consisted of either a red cross or a green tick at the centre of the screen to indicate incorrect and correct responses, respectively. This was followed by a final gap period lasting 1000 ms, 2000 ms or 3000 ms. Each feedback condition run lasted approximately 8 min. The extended third gap period in this condition ensured that all trials contained an integer number of TRs (TR = 1000 ms). This adjustment also guaranteed that the interval between the action period and the subsequent event – feedback in this condition or instruction in the response and observation conditions — was consistently 1500 ms, 2500 ms, or 3500 ms.

Although we aimed to examine the *Action* period in the response condition and the *Feedback* period in the feedback condition, we chose not to use the same runs for studying error commission and error feedback. This decision was made to avoid potential confounds, as the presence of feedback could influence how participants internally process errors.

Each run included three baseline periods, which participants were informed about in advance. These periods occurred randomly after 15, 16, or 17 trials, and consisted of white noise presented for 10 s, 11 s, or 12 s. Facial expression images of four random adult actors (two male and two female) were obtained from the Radboud Faces Database (Langner et al. 2010). Before entering the MRI scanner, participants learned the task rules and practiced by completing half a run of each condition. This ensured they understood the instructions while avoiding overtraining, which could reduce error rates during the actual experiment. The stimuli were programmed using the Psychophysics Toolbox 3.0 for MATLAB (R2018b).

At the end of the session, participants completed a questionnaire on perceived task difficulty, where they were asked to identify the most challenging cues in three categories: colour (green or red), facial expression (happy or sad), and their combination (happy green, happy red, sad green, sad red).

2.3. Data acquisition

MRI was performed using a Siemens MAGNETOM 7T Plus (Siemens, Erlangen) at Scannexus (Maastricht, The Netherlands) using a 32-channel head coil. Functional images were acquired using a 2D multiband (MB) gradient-echo echoplanar imaging (GE-EPI) sequence with the following parameters: TR/TE = 1000/21 ms, voxel size = 1.8 × 1.8 × 1.8 mm^3, 72 axial slices (whole-brain coverage), FOV = 198 × 198 mm^2, FA = 60º, phase encoding in anterior-to-posterior direction, MB factor = 4, GRAPPA in-plane acceleration factor = 2, and phase partial Fourier = 6/8. Before acquiring the functional runs, we collected 5 volumes for susceptibility distortion correction with identical settings but reversed phase encoding direction (posterior-to-anterior). A 3D whole-brain anatomical T1-weighted MP2RAGE (TR = 5000 ms, TE = 2.47 ms, 240 interleaved slices, voxel size = 0.7 × 0.7 × 0.7 mm^3) was also acquired for subsequent image registration. Cardiac data were acquired using a pulse oximeter from the physiological monitoring unit of the MRI system, while respiratory and EDA data were recorded using the BIOPAC acquisition system (BIOPAC Systems, CA) coupled with the AcqKnowledge Software (version 5.0). BIOPAC isotonic gel was applied to ensure maximum electrical conductivity between the skin and the EDA electrodes.

Electrodes were placed on the palmar surface of the right foot. This position was chosen to avoid interference from hand movements due to button pressing. Cardiac data were recorded at 400 Hz, and respiratory and EDA data were recorded at 2000 Hz. Button press information (response and response latency) was collected through two magnetic resonance compatible button boxes (one for each hand) and registered using MATLAB version R2018b.

2.4. Behavioural analysis

2.4.1. Participants' performance

To assess participants' performance, we analysed whether their responses aligned with the instruction given based on facial expression, frame colour, and frame shape cues. A correct response required an accurate integration of these cues at the correct timing, i.e., during the *Action* period (Fig. 2). Errors included incorrect button selection (e.g., pressing the right button of the left hand instead of the left button of the left hand), omission errors (i.e., no response), multiple responses (e.g., pressing the left button of the right hand followed by the left button of the left hand), anticipated and late responses (even when the given response was correct).

We measured participants' error rate, defined as the ratio between erroneous responses and the total number of required responses. We then compared this error rate across conditions involving self-generated errors (response and feedback), instructions with potentially distinct difficulty levels (happy green, happy red, sad green, and sad red) and run order, that might be associated with different learning stages. In addition to comparing error rates across conditions, we evaluated whether controlling for difficulty and learning effects was necessary in subsequent analyses.

To ensure that participants remained attentive during the observation condition runs, we also measured the error rate during catch trials.

2.4.2. Statistical analysis of behavioural data

To assess the impact of condition, instruction/difficulty, and run order/learning effect on participants' error rates, we conducted a linear mixed-effects analysis with these variables as fixed-effect predictors and error rate as the dependent variable. This approach accounted for within- and between-subject variability and allowed us to include multiple factors in the analysis (Walker et al. 2019). All main effects and their interactions were initially included, but non-significant predictors and interactions were removed to simplify the model (Seltman 2018), if the simplified model fitted as well as or better than the more complex version. Model comparisons were based on the Akaike information criterion (AIC) and the Bayesian information criterion (BIC), with preference given to models with lower values (Zhang et al. 2023). A random intercept was modelled for each participant. Results were considered significant for $p < 0.05$. We controlled for age and gender by including them as covariates in the model. The linear mixed-effects modelling was performed using IBM SPSS Statistics 27 software. Degrees of freedom in mixed models were computed using the Satterthwaite approximation implemented in SPSS. This approximation account for variance components and covariance structures, often resulting in non-

integer and large denominator degrees of freedom that reflect the number of observations rather than the number of subjects (Alnosaier 2024).

2.5. fMRI data processing

MRI data were preprocessed using BrainVoyager (version 22.4, Brain Innovation, The Netherlands) (Goebel 2012) and FMRIB Software Library (FSL, version 6.0) (Jenkinson et al. 2012), along with custom scripts written in Python (version 3.10), and MATLAB (version R2019b, MathWorks, USA). The pipeline included: (1) slice timing correction; (2) alignment of all fMRI volumes to the first volume of the first run (with trilinear interpolation for motion detection and sinc interpolation for resampling); (3) correction of geometric distortions caused by magnetic field inhomogeneity with the FSL TOPUP tool (Andersson et al. 2003); (4) temporal high-pass filtering with a cut-off frequency of 0.008 Hz; (5) inhomogeneity correction and skull stripping of the anatomical image; (6) functional and anatomical images normalization to Montreal Neurological Institute (MNI) space, including functional to anatomical image registration, and resampling of the normalised functional data to 2 mm isotropic resolution; (7) spatial smoothing with a 4 mm full-width-at-half-maximum (FWHM) isotropic Gaussian kernel; (8) estimation and high-pass filtering (cut-off frequency of 0.008 Hz) of nuisance regressors such as head motion (six motion parameters), cardiac and respiratory signals. The physiological regressors were estimated using the *physiocorr* Python library (https://github.com/BrainInnovation/physiocorr) and included RETROICOR regressors (four cardiac and four respiratory regressors) (Glover et al. 2000), heart rate variability convolved with the cardiac response function (Kassinopoulos and Mitsis 2019), and respiratory volume per time convolved with the respiratory response function (Kassinopoulos and Mitsis 2019).

2.6. fMRI data analysis

To spatially dissociate the effects of error commission, error feedback, and error observation, we employed two complementary methods. First and most importantly, we conducted a linear mixed-effects analysis to characterize the spatial evolution of error-related neural activity along the ACC using a high-resolution atlas. As a confirmatory approach, we applied a winner map analysis to identify subregions preferentially engaged by each experimental condition.

For both methods, the primary analysis involved the *Action* period (Fig. 2) for the response and observation condition runs, and the *Feedback* period in the feedback condition run. Across the entire session, we considered the following events: *instruction*, *correct trial, error trial, correct feedback, error feedback, rule change* (i.e., the moment at which some rules reversed at the middle of each run) and *catch trial*. In the response and observation condition runs, feedback events were absent; and in the response and feedback condition runs, there were no catch trials. The onset of instruction, correct feedback, error feedback, rule change, and catch trial was the moment at which these events were displayed. In the response and feedback runs, the onset of correct and error was the moment at which the button was pressed; but for the observation run, it was the moment at which the response was displayed. The onset of omission errors was estimated by calculating the mean response time for each participant within a specific condition and experimental run, then adding this value to the onset of the

action period. The durations of instruction, correct trial, error trial, correct feedback, and error feedback events were set to 1 s (corresponding to 1 TR), and the durations of the rule change and catch trials were 7 s and 3 s, respectively.

2.6.1. Study of the ACC functional parcellation based on a high-resolution atlas

We investigated how distinct ACC subregions, previously defined by a high-resolution atlas — the Yale atlas (Mcgrath et al. 2022) — respond to the different error monitoring processes studied here. Specifically, we assessed the spatial progression of error-related neural activity along the ACC. The influence of task condition (response, feedback, and observation) and performance (correct and error events) on neural activity was tested across 10 ACC subregions defined by the Yale Atlas and labelled A to J.

The single-response beta coefficients of each event were computed using the Least-Squares All (LSA) approach (Abdulrahman and Henson 2016) in SPM 12. In this approach, each correct and error event of interest — *correct trial* and *error trial* for the response and observation runs (*Action* period), and *correct feedback* and *error feedback* for the feedback runs (*Feedback* period) — was modelled as a separate regressor in the GLM. For the remaining events, all repetitions of the same type were collapsed into the same regressor, as the analysis focused solely on responses associated to correct and error events. The LSA was applied to the average time series extracted from each subregion. We then computed the single-response PSC betas by dividing each single-response beta coefficient by the run model intercept (β_0) (Mayer et al. 2012). Cardiac, respiratory, and head motion regressors were added to the design matrix as confounding signals.

As a complementary analysis, we aimed to clarify whether ACC activity associated with error commission differs depending on the presence of feedback. To address this, we assessed the influence of condition (response without feedback and response before feedback) and performance (correct vs. error events) on neural activity within the considered ACC subregions. Unlike the previous analysis, this comparison focused exclusively on the feedback and response runs and did not include feedback events, considering only the *correct trial* and *error trial* events instead (during the *Action* period). Therefore, we also computed the single-response PSC betas for *correct trial* and *error trial* events in the feedback condition, using the LSA approach (Abdulrahman and Henson 2016).

Statistical analysis

To assess the impact of condition, performance, and ACC subregion on neural activity, we conducted a linear mixed-effects model with single-response PSC betas as the dependent variable. Dummy-coded predictors representing task condition, performance, and ACC subregion were included as fixed effects, along with all possible interactions. Non-significant factors and interactions were removed to obtain the final model (Seltman 2018), if the simplified model fitted as well as or better than the more complex

version. Participant was included as a random effect, with a random intercept modelled for each participant. Linear mixed-effects models were chosen to account for within- and between-subjects variability, accommodate unequal numbers of repetitions, and allow the inclusion of multiple factors in a single model (Walker et al. 2019). Covariates, including age, gender, instruction/difficulty level, and run order/learning period were included to control for potential confounding effects. Post hoc pairwise comparisons were Bonferroni-corrected for multiple comparisons. The linear mixed-effects analyses were performed using IBM SPSS Statistics 27 software. Model assumptions (linearity, homoscedasticity, and normality of residuals) were assessed in RStudio (version 1.3.1093) using the *lme4* package.

2.6.2. Study of the ACC functional parcellation using a winner map approach

Using the winner map methodology (Schneider et al. 2019; Rosenke et al. 2021), each voxel of the ACC was attributed to the condition (response, feedback, or observation) associated with the highest statistical value (*t*-value, in this case) for the contrast *error vs. correct*.

We applied a random effects GLM (RFX GLM) analysis within the ACC using the BrainVoyager event-related deconvolution procedure with 12 data points per event. Given that a rapid event-related design was used, the hemodynamic response function (HRF) of distinct events could overlap, and the deconvolution analysis is suited to separate the contributions of different events. This procedure makes no assumptions about the HRF shape, allowing its estimation for each event type (Glover 1999). Cardiac, respiratory, and head motion regressors were added to the design matrix as confounding signals. The ACC mask was the aggregation of the Brainnetome Atlas (Fan et al. 2016) pregenual area 32 (A32p) and subgenual area 32 (A32sg). Because high-resolution anatomical parcellation was not required for this analysis, we chose the Brainnetome Atlas due to its widespread use and validation, including in our previous studies involving similar tasks (Dias et al. 2024, 2025). This approach also allowed us to perform an analysis independent from the previous one, aimed at spatially dissociating the effects of error commission, error feedback, and error observation.

Two winner maps were computed using BrainVoyager — one for the contrast *error > correct* and another for *error < correct* — to identify the winning condition (either response, feedback, or observation) for each ACC subregion. We applied a threshold of $p < 0.05$ (uncorrected), due to the exploratory nature of the analysis. We then extracted the deconvolved PSC BOLD signal for each subject and condition from the clusters identified in the winner maps. These data were used to compute the global average estimated HRF across conditions.

2.7. EDA data analysis

2.7.1. EDA data processing

Our secondary goal was to examine whether there are ACC subregions specialized in the autonomic reaction to errors. We analysed the relationship between rostroventral ACC neural activity and skin

conductance, a subset of EDA that reflects the electrical conductance of the skin. The skin conductance signal comprises two components: the slow-changing tonic component, termed skin conductance level (SCL), and the rapid-changing phasic component, or skin conductance responses (SCRs), which are rapid increases in conductance that occur on top of the tonic level. SCRs typically occur after a stimulus and are referred to as event-related SCRs, while spontaneous SCRs can also occur in the absence of specific stimulation (Yang and Huang 2024). Both SCR and SCL reflect sympathetic activity (e.g., related to stress or arousal), but while SCRs refer to transient changes in skin conductance that occur in response to specific stimuli, SCL signals the overall state of arousal (Nagai et al. 2004).

To decompose the EDA signal into tonic and phasic components, we used the SparsEDA algorithm (Hernando-gallego et al. 2018), a method based on non-negative sparse deconvolution of EDA signals, available in the Neurokit2 Python toolbox (Makowski et al. 2021). In addition, we employed Neurokit2 built-in functions for signal cleaning, peak detection, and the extraction of event-related SCRs. The event-related SCRs were extracted within a [0.5, 6] s interval following the events' onset (Figner and Murphy 2011). We included all trials (both correct and erroneous) in this analysis.

2.7.2. Statistical analysis of EDA data

To understand if error events elicit SCRs, we evaluated whether SCR frequency (computed as the ratio of SCRs elicited by an event type and the total number of such events) and amplitude were influenced by experimental conditions (response, feedback, and observation), performance (correct and error events), and their interaction. Two linear mixed-effects models were conducted – one with SCR frequency and the other with mean amplitude as the dependent variable. Condition, performance, and their interaction were included as fixed factors, while participant was considered as random variable with a random intercept. To control for potential confounders, we included covariates such as age, gender, instruction/difficulty level, and run order/learning period. Post hoc pairwise comparisons were Bonferroni-corrected for multiple comparisons. This analysis was performed using IBM SPSS Statistics 27 software.

Furthermore, to study the correlation between rostroventral ACC neural activity and the tonic and phasic components of skin conductance, we performed a standard RFX GLM analyses within the pgACC/sgACC using BrainVoyager. The model included two predictors — the phasic and tonic components of skin conductance, downsampled to match the fMRI volume TR (1 s). These components were not convolved with the HRF due to the similarity in shape and latency between the EDA response and the BOLD hemodynamic response (Leitão et al. 2020). Cardiac, respiratory, and head motion regressors were included as confounding signals. The rostroventral ACC mask was defined as the A32sg area from the Brainnetome Atlas (Fan et al. 2016). A threshold of $p < 0.05$ was applied to the group results.

3. Results

3.1. Behavioural results: participants' performance

Participants made, on average, 23.13 ± 19.47% errors in the response condition and 18.23 ± 17.43% errors in the feedback condition. A linear mixed-effects model revealed a significant influence of condition ($F(1, 150.34) = 4.19$, $p = 0.042$), run order ($F(5, 152.02) = 13.88$, $p = 3.62 \times 10^{-11}$), and instruction ($F(3, 149.91) = 12.30$, $p = 3.09 \times 10^{-7}$) on error rate (Fig. 3). We also found a significant interaction between condition and run order ($F(5, 154.71) = 3.80$, $p = 0.003$). Given the significant impact of run order and instruction on error rate, we included these variables as covariates in the following analyses to control for difficulty and learning effects.

Post hoc pairwise comparisons showed that error rates following the *happy green* and *sad green* instructions were lower than those following *happy red* and *sad red* cues (Fig. 3b), which is consistent with the rule change implied by the latter. Error rates were also compared across runs/learning periods within each condition. In the response condition, the error rate was higher in the first run compared to the subsequent runs. In the feedback condition, the first run led to a higher number of errors than the third, fifth, and sixth runs, and the number of errors in the second run was higher than the fifth and sixth runs. Supplementary Table S1 details these results.

In the observation condition, the accuracy during catch trials averaged 86.17 ± 12.77%, confirming that participants remained attentive during these runs.

Participants' ratings of task difficulty indicated that the red cue was perceived as more challenging than the green cue, and the sad cue as more challenging than the happy cue, across all participants. Overall, 90% of participants ranked the happy green instruction as the easiest, while 50% considered the happy red instruction the most difficult. Interestingly, although the red and sad cues were individually rated as more challenging, their combination (sad red) was not perceived as the most difficult. This may be because the sad red instruction represents a double reversal: when the frame is red, the easiest rule is inverted, and for sad faces, the rule is also inverted relative to happy faces. These two inversions cancel each other out, making the required response identical to the gaze direction — similar to the easiest condition (happy green). Some participants reported that this made sad red unexpectedly easier than happy red. However, this subjective perception was not reflected in the behavioural data, as happy red and sad red cues produced similar error rates.

3.2. Neurophysiological results

3.2.1. ACC functional parcellation using a high-resolution atlas

Functional differentiation between rostroventral and dorsal ACC subregions revealed by response polarity reversal

To evaluate the spatial topography of error-related neural activity along the ACC, we conducted a linear mixed-effects model to analyse the impact of condition (response, feedback, and observation), performance (correct and error events), and ACC subregion (subregions A-J) on neural activity (Fig. 4).

The model revealed significant effects of condition ($F(2, 28063.32) = 224.60$, $p = 1.69 \times 10^{-97}$) and ACC subregion ($F(9, 28070.23) = 47.75$, $p = 2.90 \times 10^{-86}$) on neural response to errors. Moreover, we found significant interactions between condition and performance ($F(2, 27948.85) = 17.74$, $p = 2.00 \times 10^{-8}$), performance and ACC subregion ($F(9, 28070.04) = 12.19$, $p = 1.88 \times 10^{-19}$), condition and ACC subregion ($F(18, 28070.04) = 45.16$, $p = 1.45 \times 10^{-158}$), and all three factors — condition, performance, and ACC subregion ($F(18, 28070.01) = 2.80$, $p = 6.56 \times 10^{-5}$).

We ran post hoc tests to compare correct and error events within each condition and ACC subregion (see Supplementary Table S2 for details). In all conditions, activity in the rostroventral subregions (corresponding to the pgACC and sgACC) was diminished following errors compared to correct actions. In the response and feedback conditions, but not in the observation condition, this pattern reversed in the dorsal subregions, with greater activity following errors. The subregions showing increased activity for errors compared to correct events in the response and feedback conditions overlapped, although the feedback condition showed correct vs. error differences across a larger number of subregions than the response condition.

Error-related ACC activity appears to be unaffected by feedback during error commission

To clarify whether ACC activity related to error commission (during the *Action* period) differs depending on the presence of feedback, we assessed the influence of condition (response without feedback and response before feedback), performance (correct and error events), and ACC subregion on neural activity using a linear mixed-effects model.

This analysis showed significant effects of condition ($F(1, 18998.70) = 21.97$, $p = 2.79 \times 10^{-6}$) and ACC subregion ($F(9, 18998.08) = 199.25$, $p < < 0.001$) on neural activity. Additionally, there were significant interactions between condition and ACC subregion ($F(9, 18998.05) = 2.84$, $p = 0.002$), as well as between performance and ACC subregion ($F(10, 18996.34) = 5.45$, $p = 3.98 \times 10^{-6}$).

Post hoc tests revealed that ACC activity associated with responses without subsequent feedback was higher than that associated with responses preceding upcoming feedback in subregions C, E, F, G, and H, whereas the opposite pattern was observed in subregion A. Furthermore, ACC activity following errors was reduced compared to correct events in subregions A and E, but was greater after errors than correct events in subregions H and I, regardless of condition. Importantly, the differences between correct and error events across subregions were similar in both conditions, as no significant interaction between condition and performance was found. Detailed results are provided in Supplementary Figure S1 and Supplementary Table S3.

3.2.2. ACC functional parcellation using winner maps confirms distinct subregions for self-generated and observed errors

To further investigate which ACC subregions were predominantly engaged during error commission, error feedback, and error observation, we applied a second confirmatory approach — a winner map analysis. With this method, each ACC voxel was assigned to the condition — response, feedback, or observation — that exhibited the highest statistical value for the contrast between error and correct trials. The winner maps (shown in Supplementary Fig. S2) revealed clusters with increased dACC activity following errors compared to correct actions in the response and feedback conditions. In contrast, the observation condition showed diminished ACC activity (primarily in the pgACC, extending into the sgACC and dACC) following errors compared to correct actions. In the pgACC, clusters of decreased activity following errors relative to correct events were observed across all conditions (details in Supplementary Table S4).

Supplementary Figure S2B displays the ROI-specific ACC hemodynamic responses for all conditions (response, feedback, and observation). For each condition, the largest cluster from the contrasts *error > correct* and *error < correct* was selected, and its hemodynamic response across all conditions is illustrated. We can verify that the ACC activity associated with the response condition closely resembled that of the feedback condition but largely differed from the observation condition. Supplementary Figure S3 shows the ACC hemodynamic responses of the remaining clusters.

3.3. EDA results: pgACC subregions associated with autonomic response to errors

To examine the relationship between our task and SCRs, we first assessed whether SCR frequency and amplitude were influenced by the error monitoring condition (response, feedback, observation), participants' performance (correct vs. error events), or their interaction. Linear mixed-effects models revealed no significant effects on either measure. Average SCR frequencies and amplitudes for correct and error trials across all conditions are presented in Supplementary Table S5.

Additionally, to investigate the neural correlates of the autonomic error processing within the rostroventral ACC, we analysed the pgACC/sgACC correlates of tonic and phasic components of skin conductance. BOLD activity correlated with these components in the pgACC, but not in the sgACC, suggesting that the latter might not contribute to autonomic processing in this specific context. Specifically, the phasic component showed a positive relationship with pgACC activity, whereas the tonic component exhibited an inverse relationship. Group correlation maps are displayed in Supplementary Figure S4, and details about the ACC clusters associated with the EDA signal are provided in Supplementary Table S6.

4. Discussion

In this study, we investigated the functional parcellation of the ACC during error monitoring. Using a complex set of tasks, we compared the effects of error commission, error feedback, and error observation on ACC activity. Our findings revealed a functional segregation between the pgACC/sgACC

compartments and the dACC, identified through a reversal in response polarity between errors and correct trials.

Participants learned the task, as evidenced by a significant decrease in error rates from the first to subsequent experimental runs. Additionally, error rates varied across instruction types, verifying the existence of different difficulty levels, as also reported by participants and our previous studies using a similar task (Dias et al. 2024, 2025).

Overall, mapping of the ACC revealed distinct subregion recruitment during different forms of error monitoring. First, dACC activity increased following self-generated errors (in the response and feedback conditions) compared to correct actions, but no significant differences were found in the observation condition. Second, BOLD activity in the rostroventral ACC areas (corresponding to the pgACC and sgACC) was reduced for errors relative to correct events across all error monitoring processes, with the most pronounced and widespread reduction occurring in the observation condition. Third, although the ACC subregions showing greater activity following errors than correct actions in the response and feedback conditions overlapped, the area activated by the feedback condition was larger. These findings were revealed through two independent analyses.

As previously mentioned, in all error monitoring processes, activity in the rostroventral ACC subregions was lower following errors compared to correct actions. In the response and feedback conditions, but not in the observation condition, this pattern was reversed in the dorsal subregions, with greater activity following errors. These results support previous studies suggesting a functional distinction between the sgACC/pgACC and dACC. On the one hand, Bush et al. (2000) suggested a broad division within the ACC, with the rostroventral “affective” regions (including the pgACC and sgACC) being activated by emotional tasks and deactivated by cognitively demanding tasks, while the dorsal “cognitive” regions (dACC) exhibit the opposite pattern. Translating this interpretation to our findings, the rostroventral ACC response may represent the socioemotional aspects of error monitoring, most prominent during error judgement, whereas the dACC activity may reflect the cognitive aspects of error monitoring, more evident during error commission and processing (Shane et al. 2008; Marinkovic and Rosen 2022). On the other hand, a review by Grabenhorst and Rolls (2011) proposed that the sgACC and pgACC respond to pleasant stimuli, whereas the dACC processes unpleasant stimuli. Similarly, a review by Liu et al. (2011) associated the sgACC/pgACC with positive rewards and the dACC with negative rewards. Our finding of a correct/error dissociation aligns with these pleasant/unpleasant and positive/negative divisions. Importantly, to the best of our knowledge, this study is the first to demonstrate ACC parcellation based on a reversal in response polarity across subregions.

Among all conditions, the feedback condition provides the clearest functional delineation between the pgACC and dACC — whose boundary is imprecisely defined in the literature (Tang et al. 2019) — as it elicited the most pronounced contrast. This is unsurprising, as activity following external feedback reflects certainty about the outcome, whereas activity following internal judgment primarily indicates confidence in the action taken.

Beyond their link to emotions, pleasant stimuli, and positive rewards, the sgACC and pgACC have also been implicated in processing social (Lockwood et al. 2016; Will et al. 2017) and “other-referential” information (Shane et al. 2008). For instance, Lockwood et al. (2016) demonstrated that the sgACC encodes prediction errors — differences between predicted and obtained outcomes — but only when rewards benefit others, with stronger activity observed in empathic individuals. These findings agree with the involvement of the sgACC and pgACC in the error observation process revealed in the current study.

A surprising finding was the absence of differences in dACC activity between correct and erroneous events in the observation condition, contrasting with the patterns observed for the response and feedback conditions. While previous studies have suggested that error commission and error observation share common neural mechanisms (Ninomiya et al. 2018), this lack of differentiation may relate to the irrelevance of the observed outcomes to the observer's goals. Musco et al. (2023) proposed that observational error monitoring is influenced by the extent to which the other’s outcomes affect the observer’s objectives. Supporting this, de Bruijn et al. (2007) found no oERN during the observation of erroneous everyday actions, and suggested that this component is only elicited when the observed error has direct consequences for personal adjustments. Similarly, Koban et al. (2010) showed that the oERN varied depending on social contexts (cooperation vs. competition) and relational factors like sympathy with the other player. Moreover, Fukushima and Hiraki (2009) reported that the oERN was significantly elicited only when observing the outcomes of decisions made by humans, with higher amplitudes linked to increased empathy levels. Moreover, the absence of dACC distinction between correct and erroneous events in the observation condition aligns with theories postulating that, rather than detecting errors, the dACC is implicated in action selection (Holroyd and Coles 2008), triggering post-error adjustments and recruiting cognitive control following errors (Shenhav et al. 2013). Given this context, one possible interpretation of our findings is that, since participants did not make behavioural adjustments in the observation condition, dACC activity did not increase following errors.

As previously mentioned, we observed an overlap between the regions activated by error commission and error feedback, with a larger area engaged during error feedback. This overlap may reflect the functional similarity between these processes and aligns with studies suggesting that both error commission and error feedback recruit the same dACC subregions (Holroyd et al. 2004; Gruendler et al. 2011). However, the broader activation observed in the feedback condition may indicate additional processing demands, such as evaluating externally provided information. Despite the overlap, the two conditions exhibited distinct activation patterns across ACC subregions: in the response condition, BOLD activity generally increased along a rostroventral-to-dorsal axis, whereas in the feedback condition, activity showed an initial increase followed by an abrupt decrease.

Previous studies have demonstrated that the ERN is elicited when internal information is sufficient to recognize an erroneous response, whereas the FRN emerges only when external feedback provides additional necessary information (Heldmann et al. 2008; Gentsch et al. 2009). In the present study, the ACC activated following both error commission and error feedback, suggesting that internal information was sufficient for error detection, with external feedback serving as confirmatory input. We also

compared ACC activity between error commission without feedback and error commission followed by feedback. Correct and error events showed similar differential activation patterns across conditions. Even so, ACC activity during responses without subsequent feedback was generally higher than during responses followed by feedback. This finding may reflect reduced ACC engagement when internal information about action outcomes is less critical. Notably, ACC activity was already present immediately after error commission, even when feedback was provided later. This suggests that error processing was initiated internally upon response execution, rather than being dependent on external feedback. Such early ACC engagement may support faster post-error adjustments.

Given the reported role of the ACC in autonomic regulation (Beissner et al. 2013; Seamans and Floresco 2022), and the link between error processing and changes in skin conductance (Hajcak et al. 2003), we examined whether specific ACC subregions have a role in supporting the autonomic response to errors, as assessed via skin conductance measurements. We found a correlation between the phasic and tonic components of the skin conductance signal and neural activity in the pgACC. Specifically, the phasic component showed a positive relationship with pgACC activity, whereas the tonic component exhibited an inverse relationship. Nagai et al. (2004) similarly investigated the neural correlates of skin conductance components, reporting a comparable correlation directionally but distinct specialized subregions. Their findings indicated that dACC activity, extending into the pgACC, was positively correlated with the phasic component, whereas sgACC activation was negatively correlated with the tonic component. It should be noted that our analysis was conducted without correction for multiple comparisons and involved a small sample size, and thus these findings should be interpreted with caution. Nonetheless, our results suggest that autonomic processing in this type of task may provide an additional functional separation between the pgACC and sgACC, as the sgACC did not exhibit this pattern of correlation. Future studies are needed to further investigate the functional significance of this dissociation.

All these findings shed light on the functional organization of the ACC and its role during distinct error monitoring processes. This study highlights the distinction between rostroventral and dorsal ACC subregions. The dorsal areas appear to be involved in the cognitive aspects of error monitoring, essential for behavioural adjustments and learning from errors — processes most prominent during error commission and processing. In contrast, the rostroventral ACC may be more engaged in the socioemotional processes of error monitoring, necessary for recognizing errors made by others.

4.1. Limitations of the study

Our study has some limitations. Given the present sample size, our findings should be considered preliminary and require replication in a larger cohort. At the same time, the ACC exhibits substantial interindividual variability, and group-level analyses may mix signals from different subregions, potentially obscuring meaningful functional differences (Ullsperger 2017; Smith et al. 2021). To address this, future research should include multiple sessions per participant to ensure sufficient data for single-subject analyses. Besides, to verify whether the absence of dACC activity during the error observation condition

resulted from the irrelevance of observed outcomes to the observer's goals, future studies should adapt the task to manipulate this characteristic. Finally, combining EEG and fMRI would provide valuable insights by enabling a direct comparison of the neural correlates of the ERN, FRN, and oERN within the ACC.

Declarations

Competing interests

The authors have no relevant financial or non-financial interests to disclose.

Ethics approval

This study was performed in line with the principles of the Declaration of Helsinki. Approval was granted by the Ethics Review Committee of the Faculty of Psychology and Neuroscience of Maastricht University (approval reference: OZL_253_75_05_2022).

Consent to participate

Informed consent was obtained from all individual participants included in the study.

Funding

This work was supported by FCT Portuguese National Funding Agency for Science, Research and Technology (grants UIDB/4950/2020 and 2025, https://doi.org/10.54499/UIDB/04950/2020; UIDP/4950/2020 and 2025, https://doi.org/10.54499/UIDP/04950/2020; 10.54499/UI/BD/150832/2021, https://doi.org/10.54499/UI/BD/150832/2021).

Author Contribution

C. Dias, T. Sousa, M. Lührs, R. Goebel and M. Castelo-Branco conceived and designed the experiment. C. Dias and A. Ciarlo performed the experiment and acquired the data. All authors contributed to the analysis and interpretation of the results. C. Dias wrote the first draft of the manuscript and prepared figures and tables. All authors reviewed drafts of the paper and approved the final manuscript.

Acknowledgments

We are very grateful to the participants who enrolled in this study.

Data Availability

MRI data have been deposited at OpenNeuro and are publicly available at https://openneuro.org/datasets/ds006550.All original code has been deposited at GitHub and is publicly available at https://github.com/CIBIT-UC/ACC_subregions_errorMonitoring.

References

1. Abdulrahman H, Henson RN (2016) Effect of trial-to-trial variability on optimal event-related fMRI design: Implications for Beta-series correlation and multi-voxel pattern analysis. Neuroimage 125:756–766. https://doi.org/10.1016/j.neuroimage.2015.11.009
2. Alexander L, Jelen LA, Mehta MA, Young AH (2021) The anterior cingulate cortex as a key locus of ketamine's antidepressant action. Neurosci Biobehav Rev 127:531–554. https://doi.org/10.1016/j.neubiorev.2021.05.003
3. Alnosaier W (2024) Comparisons of the Satterthwaite Approaches for Fixed Effects in Linear Mixed Models. Int J Stat Probab 13:22–39. https://doi.org/10.5539/ijsp.v13n1p22
4. Andersson JLR, Skare S, Ashburner J (2003) How to correct susceptibility distortions in spin-echo echo-planar images: application to diffusion tensor imaging. Neuroimage 20:870–888. https://doi.org/10.1016/S1053-8119(03)00336-7
5. Apps MAJ, Ramnani N (2014) The Anterior Cingulate Gyrus Signals the Net Value of Others' Rewards. J Neurosci 34:6190–6200. https://doi.org/10.1523/JNEUROSCI.2701-13.2014
6. Beckmann M, Johansen-Berg H, Rushworth MFS (2009) Connectivity-based parcellation of human cingulate cortex and its relation to functional specialization. J Neurosci 29:1175–1190. https://doi.org/10.1523/JNEUROSCI.3328-08.2009
7. Beissner F, Meissner K, Bär K-J, Napadow V (2013) The Autonomic Brain: An Activation Likelihood Estimation Meta-Analysis for Central Processing of Autonomic Function. J Neurosci 33:10503–10511. https://doi.org/10.1523/JNEUROSCI.1103-13.2013
8. Bhattacharyya S, Konar A, Tibarewala DN, Hayashibe M (2017) A generic transferable EEG decoder for online detection of error potential in target selection. Front Neurosci 11:226. https://doi.org/10.3389/fnins.2017.00226
9. Boly M, Gosseries O, Massimini M, Rosanova M (2016) Functional Neuroimaging Techniques. In: The Neurology of Consciousness. Elsevier Ltd, pp 31–47
10. Bush G, Luu P, Posner MI (2000) Cognitive and emotional influences in anterior cingulate cortex. Trends Cogn Sci 4:215–222. https://doi.org/10.1016/s1364-6613(00)01483-2
11. Chavarriaga R, Sobolewski A, Millán J del R (2014) Errare machinale est: the use of error-related potentials in brain-machine interfaces. Front Neurosci 8:208. https://doi.org/10.3389/fnins.2014.00208

12. De Bruijn ERA, Schubotz RI, Ullsperger M (2007) An event-related potential study on the observation of erroneous everyday actions. Cogn Affect Behav Neurosci 7:278–285. https://doi.org/10.3758/cabn.7.4.278
13. Dejanović I, Dejanović M, Vidaković J, Nikolić S (2021) PyFlies : A Domain-Specific Language for Designing Experiments in Psychology. Appl Sci 11:. https://doi.org/10.3390/app11177823
14. Dias C, Sousa T, Castelo-branco M (2024) A chronometric relationship between circuits underlying learning and error monitoring in the basal ganglia and salience network. Imaging Neurosci 2:imag–2–00343. https://doi.org/10.1162/imag_a_00343
15. Dias C, Sousa T, Mouga S, Castelo-branco M (2025) A link between error monitoring and basal ganglia-dependent learning in autism. Brain Commun 7:fcaf414. https://doi.org/10.1093/braincomms/fcaf414
16. Dixon ML, Thiruchselvam R, Todd R, Christoff K (2017) Emotion and the Prefrontal Cortex: An Integrative Review. Psychol Bull 143:1033–1081. https://doi.org/10.1037/bul0000096
17. Estiveira J, Dias C, Costa D, et al (2022) An Action-Independent Role for Midfrontal Theta Activity Prior to Error Commission. Front Hum Neurosci 16:805080. https://doi.org/10.3389/fnhum.2022.805080
18. Fan L, Li H, Zhuo J, et al (2016) The Human Brainnetome Atlas: A New Brain Atlas Based on Connectional Architecture. Cereb Cortex 26:3508–3526. https://doi.org/10.1093/cercor/bhw157
19. Fidêncio AX, Klaes C, Iossifidis I (2022) Error-Related Potentials in Reinforcement Learning-Based Brain-Machine Interfaces. Front Hum Neurosci 16:806517. https://doi.org/10.3389/fnhum.2022.806517
20. Figner B, Murphy RO (2011) Using skin conductance in judgment and decision making research. In: A handbook of process tracing methods for decision research: A critical review and user's guide. Psychology Press, pp 163–184
21. Fu Z, Sajad A, Errington SP, et al (2023) Neurophysiological mechanisms of error monitoring in human and non-human primates. Nat Rev Neurosci 24:153–172. https://doi.org/10.1038/s41583-022-00670-w
22. Fukushima H, Hiraki K (2009) Whose loss is it? Human electrophysiological correlates of non-self reward processing. Soc Neurosci 4:261–275. https://doi.org/10.1080/17470910802625009
23. Gentsch A, Ullsperger P, Ullsperger M (2009) Dissociable medial frontal negativities from a common monitoring system for self- and externally caused failure of goal achievement. Neuroimage 47:2023–2030. https://doi.org/10.1016/j.neuroimage.2009.05.064
24. Glover GH (1999) Deconvolution of Impulse Response in Event-Related BOLD fMRI. Neuroimage 9:416–429. https://doi.org/10.1006/nimg.1998.0419
25. Glover GH, Li TQ, Ress D (2000) Image-based method for retrospective correction of physiological motion effects in fMRI: RETROICOR. Magn Reson Med 44:162–167. https://doi.org/10.1002/1522-2594

26. Goebel R (2012) BrainVoyager — Past, present, future. Neuroimage 62:748–756. https://doi.org/10.1016/j.neuroimage.2012.01.083
27. Grabenhorst F, Rolls ET (2011) Value, pleasure and choice in the ventral prefrontal cortex. Trends Cogn Sci 15:56–67. https://doi.org/10.1016/j.tics.2010.12.004
28. Gruendler TOJ, Ullsperger M, Huster RJ (2011) Event-Related Potential Correlates of Performance-Monitoring in a Lateralized Time-Estimation Task. PLoS One 6:e25591. https://doi.org/10.1371/journal.pone.0025591
29. Hajcak G, McDonald N, Simons RF (2003) To err is autonomic: Error-related brain potentials, ANS activity, and post-error compensatory behavior. Psychophysiology 40:895–903. https://doi.org/10.1111/1469-8986.00107
30. Heilbronner SR, Hayden BY (2016) Dorsal Anterior Cingulate Cortex: A Bottom-Up View. Annu Rev Neurosci 39:149–170. https://doi.org/10.1146/annurev-neuro-070815-013952
31. Heldmann M, Rüsseler J, Münte TF (2008) Internal and external information in error processing. BMC Neurosci 9:. https://doi.org/10.1186/1471-2202-9-33
32. Hernando-gallego F, Luengo D, Art A (2018) Feature Extraction of Galvanic Skin Responses by Nonnegative Sparse Deconvolution. IEEE J Biomed Heal Informatics 22:1385–1394. https://doi.org/10.1109/JBHI.2017.2780252
33. Holper L, Jäger N, Scholkmann F, Wolf M (2013) Error detection and error memory in spatial navigation as reflected by electrodermal activity. Cogn Process 14:377–389. https://doi.org/10.1007/s10339-013-0567-z
34. Holroyd CB, Coles MGH (2008) Dorsal anterior cingulate cortex integrates reinforcement history to guide voluntary behavior. Cortex 44:548–559. https://doi.org/10.1016/J.CORTEX.2007.08.013
35. Holroyd CB, Nieuwenhuis S, Yeung N, et al (2004) Dorsal anterior cingulate cortex shows fMRI response to internal and external error signals. Nat Neurosci 7:497–498. https://doi.org/10.1038/nn1238
36. Jahn A, Nee DE, Alexander WH, Brown JW (2014) Distinct regions of anterior cingulate cortex signal prediction and outcome evaluation. Neuroimage 95:80–89. https://doi.org/10.1016/j.neuroimage.2014.03.050
37. Jenkinson M, Beckmann CF, Behrens TEJ, et al (2012) FSL. Neuroimage 62:782–790. https://doi.org/10.1016/j.neuroimage.2011.09.015
38. Kassinopoulos M, Mitsis GD (2019) Identification of physiological response functions to correct for fluctuations in resting-state fMRI related to heart rate and respiration. Neuroimage 202:116150. https://doi.org/10.1016/j.neuroimage.2019.116150
39. Koban L, Pourtois G, Vocat R, Vuilleumier P (2010) When your errors make me lose or win: event-related potentials to observed errors of cooperators and competitors. Soc Neurosci 5:360–374. https://doi.org/10.1080/17470911003651547
40. Kolling N, Wittmann MK, Behrens TEJ, et al (2016) Value, search, persistence and model updating in anterior cingulate cortex. Nat Neurosci 19:1280–1285. https://doi.org/10.1038/nn.4382

41. Langner O, Dotsch R, Bijlstra G, et al (2010) Presentation and validation of the radboud faces database. Cogn Emot 24:1377–1388. https://doi.org/10.1080/02699930903485076
42. Leitão J, Meuleman B, van De Ville D, Vuilleumier P (2020) Computational imaging during video game playing shows dynamic synchronization of cortical and subcortical networks of emotions. PLoS Biol 18:e3000900. https://doi.org/10.1371/journal.pbio.3000900
43. Liu X, Hairston J, Schrier M, Fan J (2011) Common and distinct networks underlying reward valence and processing stages: A meta-analysis of functional neuroimaging studies. Neurosci Biobehav Rev 35:1219–1236. https://doi.org/10.1016/j.neubiorev.2010.12.012
44. Lockwood PL, Apps MAJ, Valton V, et al (2016) Neurocomputational mechanisms of prosocial learning and links to empathy. PNAS 113:9763–9768. https://doi.org/10.1073/pnas.1603198113
45. Lockwood PL, Wittmann MK, Apps MAJ, et al (2018) Neural mechanisms for learning self and other ownership. Nat Commun 9:4747. https://doi.org/10.1038/s41467-018-07231-9
46. Makowski D, Pham T, Lau ZJ, et al (2021) NeuroKit2: A Python toolbox for neurophysiological signal processing. Behav Res Methods 53:1689–1696. https://doi.org/10.3758/s13428-020-01516-y
47. Marinkovic K, Rosen BQ (2022) Theta oscillatory dynamics of inhibitory control, error processing, and post-error adjustments: Neural underpinnings and alcohol-induced dysregulation in social drinkers. Alcohol Clin Exp Res 46:1220–1232. https://doi.org/10.1111/acer.14856
48. Mayer AR, Teshiba TM, Franco AR, et al (2012) Modeling conflict and error in the medial frontal cortex. Hum Brain Mapp 33:2843–2855. https://doi.org/10.1002/hbm.21405
49. Mcgrath H, Zaveri HP, Collins E, et al (2022) High-resolution cortical parcellation based on conserved brain landmarks for localization of multimodal data to the nearest centimeter. Sci Rep 12:18778. https://doi.org/10.1038/s41598-022-21543-3
50. Musco MA, Zazzera E, Paulesu E, Sacheli LM (2023) Error observation as a window on performance monitoring in social contexts? A systematic review. Neurosci Biobehav Rev 147:105077. https://doi.org/10.1016/j.neubiorev.2023.105077
51. Nagai Y, Critchley HD, Featherstone E, et al (2004) Activity in ventromedial prefrontal cortex covaries with sympathetic skin conductance level: a physiological account of a “default mode” of brain function. Neuroimage 22:243–251. https://doi.org/10.1016/j.neuroimage.2004.01.019
52. Ninomiya T, Noritake A, Ullsperger M, Isoda M (2018) Performance monitoring in the medial frontal cortex and related neural networks: From monitoring self actions to understanding others’ actions. Neurosci Res 137:1–10. https://doi.org/10.1016/j.neures.2018.04.004
53. Oldfield RC (1971) The assessment and analysis of handedness: The Edinburgh inventory. Neuropsychologia 9:97–113. https://doi.org/10.1016/0028-3932(71)90067-4
54. Picard N, Strick PL (1996) Motor Areas of the Medial Wall: A Review of Their Location and Functional Activation. Cereb Cortex 6:342–353. https://doi.org/10.1093/cercor/6.3.342
55. Rosenke M, van Hoof R, van der Hurk J, et al (2021) A Probabilistic Functional Atlas of Human Occipito-Temporal Visual Cortex. Cereb Cortex 31:603–619. https://doi.org/10.1093/cercor/bhaa246

56. Sakata H, Kim Y, Nejime M, et al (2019) Laminar Pattern of Projections Indicates the Hierarchical Organization of the Anterior Cingulate-Temporal Lobe Emotion System. Front Neuroanat 13:. https://doi.org/10.3389/fnana.2019.00074
57. Schneider CL, Prentiss EK, Busza A, et al (2019) Survival of retinal ganglion cells after damage to the occipital lobe in humans is activity dependent. Proc R Soc B 286:20182733. https://doi.org/10.1098/rspb.2018.2733
58. Seamans JK, Floresco SB (2022) Event-based control of autonomic and emotional states by the anterior cingulate cortex. Neurosci Biobehav Rev 133:104503. https://doi.org/10.1016/j.neubiorev.2021.12.026
59. Seltman HJ (2018) Mixed Models. In: Experimental Design And Analysis. pp 357–378
60. Shane MS, Stevens M, Harenski CL, Kiehl KA (2008) Neural correlates of the processing of another's mistakes: A possible underpinning for social and observational learning. Neuroimage 42:450–459. https://doi.org/10.1016/j.neuroimage.2007.12.067
61. Shenhav A, Botvinick MM, Cohen JD (2013) The expected value of control: An integrative theory of anterior cingulate cortex function. Neuron 79:217–240. https://doi.org/10.1016/j.neuron.2013.07.007
62. Shenhav A, Straccia MA, Musslick S, et al (2018) Dissociable neural mechanisms track evidence accumulation for selection of attention versus action. Nat Commun 9:. https://doi.org/10.1038/s41467-018-04841-1
63. Silk JS, Sequeira SS, Jones NP, et al (2022) Subgenual Anterior Cingulate Cortex Reactivity to Rejection Vs. Acceptance Predicts Depressive Symptoms among Adolescents with an Anxiety History. J Clin Child Adolesc Psychol. https://doi.org/10.1080/15374416.2021.2019048
64. Smith DM, Perez DC, Porter A, et al (2021) Light through the fog: using precision fMRI data to disentangle the neural substrates of cognitive control. Curr Opin Behav Sci 40:19–26. https://doi.org/10.1016/j.cobeha.2020.12.004
65. Stevens FL, Hurley RA, Taber KH (2011) Anterior Cingulate Cortex: Unique Role in Cognition and Emotion. J Neuropsychiatry Clin Neurosci 23:. https://doi.org/10.1176/jnp.23.2.jnp121
66. Tang W, Jbabdi S, Zhu Z, et al (2019) A connectional hub in the rostral anterior cingulate cortex links areas of emotion and cognitive control. Elife 8:e43761. https://doi.org/10.7554/eLife.43761
67. Ullsperger M (2017) Neural Bases of Performance Monitoring. In: Egner T (ed) The Wiley Handbook of Cognitive Control, First. John Wiley & Sons, Ltd, pp 292–313
68. Ullsperger M, Danielmeier C, Jocham G (2014) Neurophysiology of performance monitoring and adaptive behavior. Physiol Rev 94:35–79. https://doi.org/10.1152/physrev.00041.2012
69. Vogt BA (2016) Midcingulate cortex: Structure, connections, homologies, functions and diseases. J Chem Neuroanat 74:28–46. https://doi.org/10.1016/j.jchemneu.2016.01.010
70. Vogt BA (2005) Pain and emotion interactions in subregions of the cingulate gyrus. Nat Rev 6:533–544. https://doi.org/10.1038/nrn1704

71. Walker EA, Redfern A, Oleson JJ (2019) Linear mixed-model analysis to examine longitudinal trajectories in vocabulary depth and breadth in children who are hard of hearing. J Speech, Lang Hear Res 62:525–542. https://doi.org/10.1044/2018_JSLHR-L-ASTM-18-0250
72. Weiss AR, Gillies MJ, Philiastides MG, et al (2018) Dorsal Anterior Cingulate Cortices Differentially Lateralize Prediction Errors and Outcome Valence in a Decision-Making Task. Front Hum Neurosci 12:. https://doi.org/10.3389/fnhum.2018.00203
73. Will G, Rutledge RB, Moutoussis M, Dolan RJ (2017) Neural and computational processes underlying dynamic changes in self-esteem. Elife 6:e28098. https://doi.org/10.7554/eLife.28098
74. Yang M, Huang J (2024) Phasic and tonic electrodermal activity in emotional responses to acoustic environments. J Environ Psychol 96:102282. https://doi.org/10.1016/j.jenvp.2024.102282
75. Yu C, Zhou Y, Liu Y, et al (2011) Functional segregation of the human cingulate cortex is confirmed by functional connectivity based neuroanatomical parcellation. Neuroimage 54:2571–2581. https://doi.org/10.1016/j.neuroimage.2010.11.018
76. Zhang J, Yang Y, Ding J (2023) Information criteria for model selection. Wiley Interdiscip Rev Comput Stat 15:e1607. https://doi.org/10.1002/wics.1607
77. Zhou Z, Gao Y, Bao W, et al (2024) Distinctive intrinsic functional connectivity alterations of anterior cingulate cortex subdivisions in major depressive disorder: A systematic review and meta-analysis. Neurosci Biobehav Rev 159:105583. https://doi.org/10.1016/j.neubiorev.2024.105583

Figures

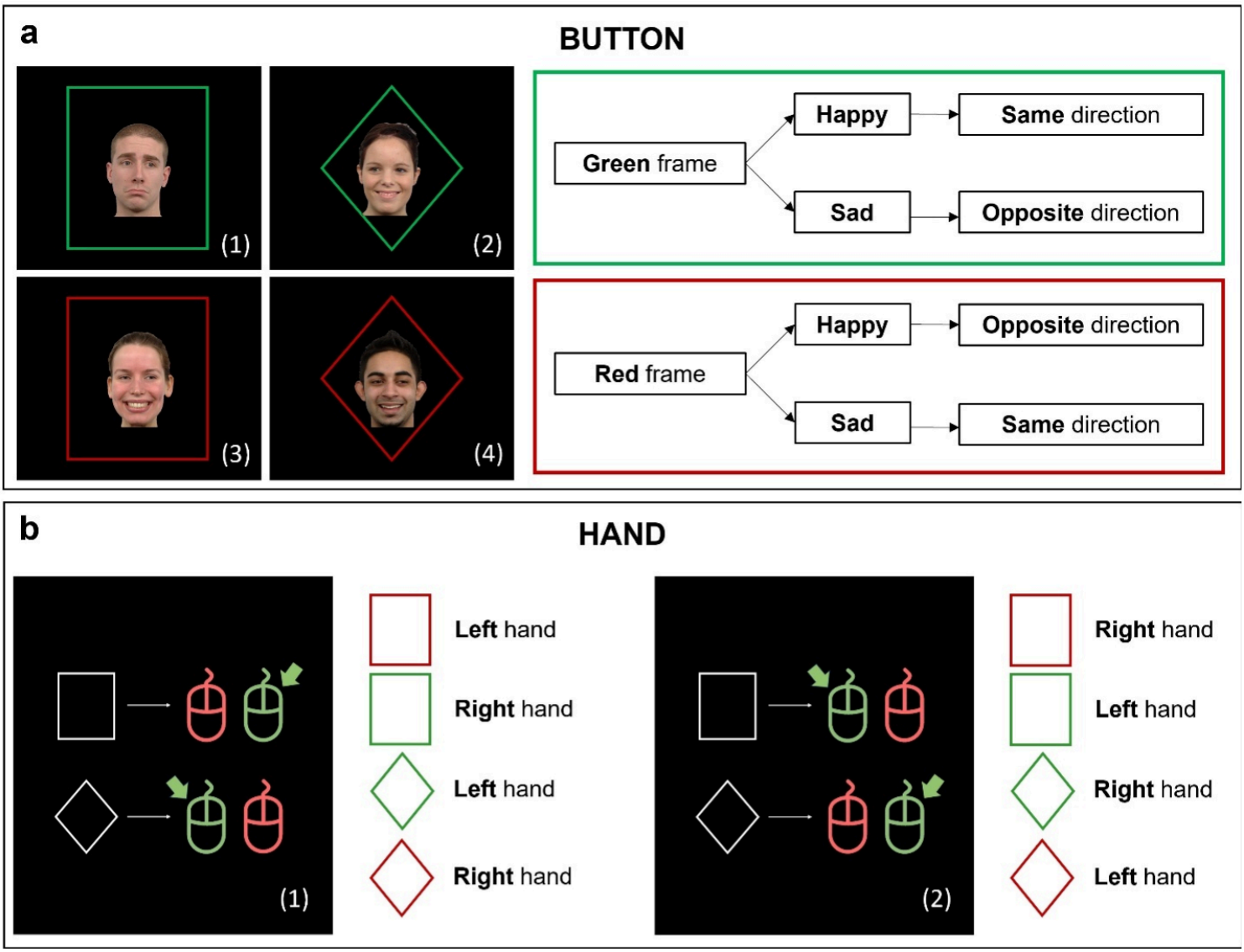


Figure 1

Experimental task summary. In this task, there were four possible responses (left-click using the left hand, right-click using the left hand, left-click using the right hand, and right-click using the right hand) that depended on the correct integration of four cues (emotional expression, gaze direction, frame shape, and frame colour) and additional information provided at the beginning and middle of each run. (a) If the frame was green, a happy face indicated to click in the direction of the face's eye gaze, and a sad face indicated to click in the opposite direction of the face's eye gaze; if the frame was red, the instructions were reversed. (b) To choose the correct hand, participants had to integrate the frame colour and frame shape cues with the information from one of these two schematics with a black background. One schematic was presented at the beginning of each run, and the other was introduced midway, reversing the response rules. According to the first schematic (bottom left panel), a green rectangle or red diamond indicated a right-hand response, while a red rectangle or green diamond indicated a left-hand response. For instance, according to the first schematic, the correct responses for the examples illustrated in (A) would be (1) to press the left button of the right hand, and (2) to press the left button of the left hand, (3) to press the left button of the left hand, and (4) to press the left button of

the right hand. These rules applied to all three task variations (focusing on error commission, feedback processing, and error observation). Facial expression stimuli were sourced from the Radboud Faces Database (Langner et al. 2010). Adapted from Dias et al. (2024, 2025) under the Creative Commons Attribution 4.0 International (CC BY 4.0) license

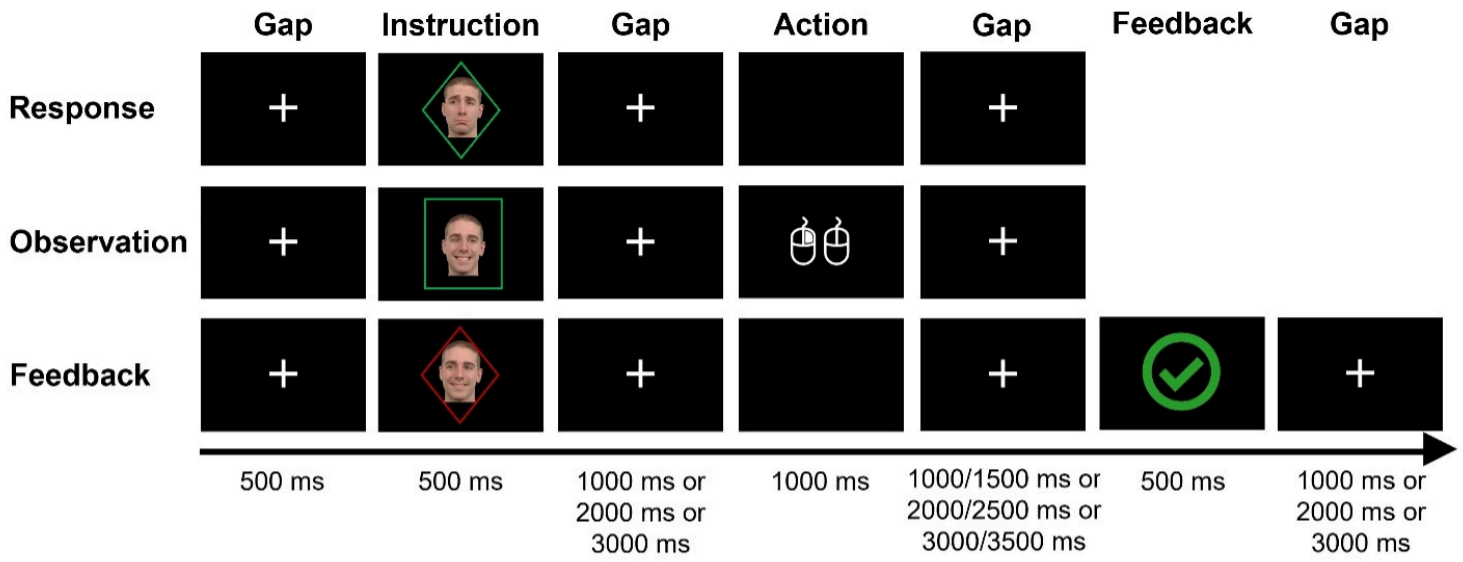


Figure 2

Experimental design. In the response and observation conditions, each trial consisted of the instruction and action periods interleaved with three gaps. In the response condition, the action period displayed a black background during which participants should press the chosen button. In the observation condition, one of four possible responses was displayed. In this case, the right-click with the left hand was the response shown. The feedback condition was similar to the response condition but included additional feedback on participants' performance and a fourth gap period. Facial expression stimuli were sourced from the Radboud Faces Database (Langner et al. 2010). Adapted from Dias et al. (2024, 2025) under Creative Commons Attribution 4.0 International (CC BY 4.0) license

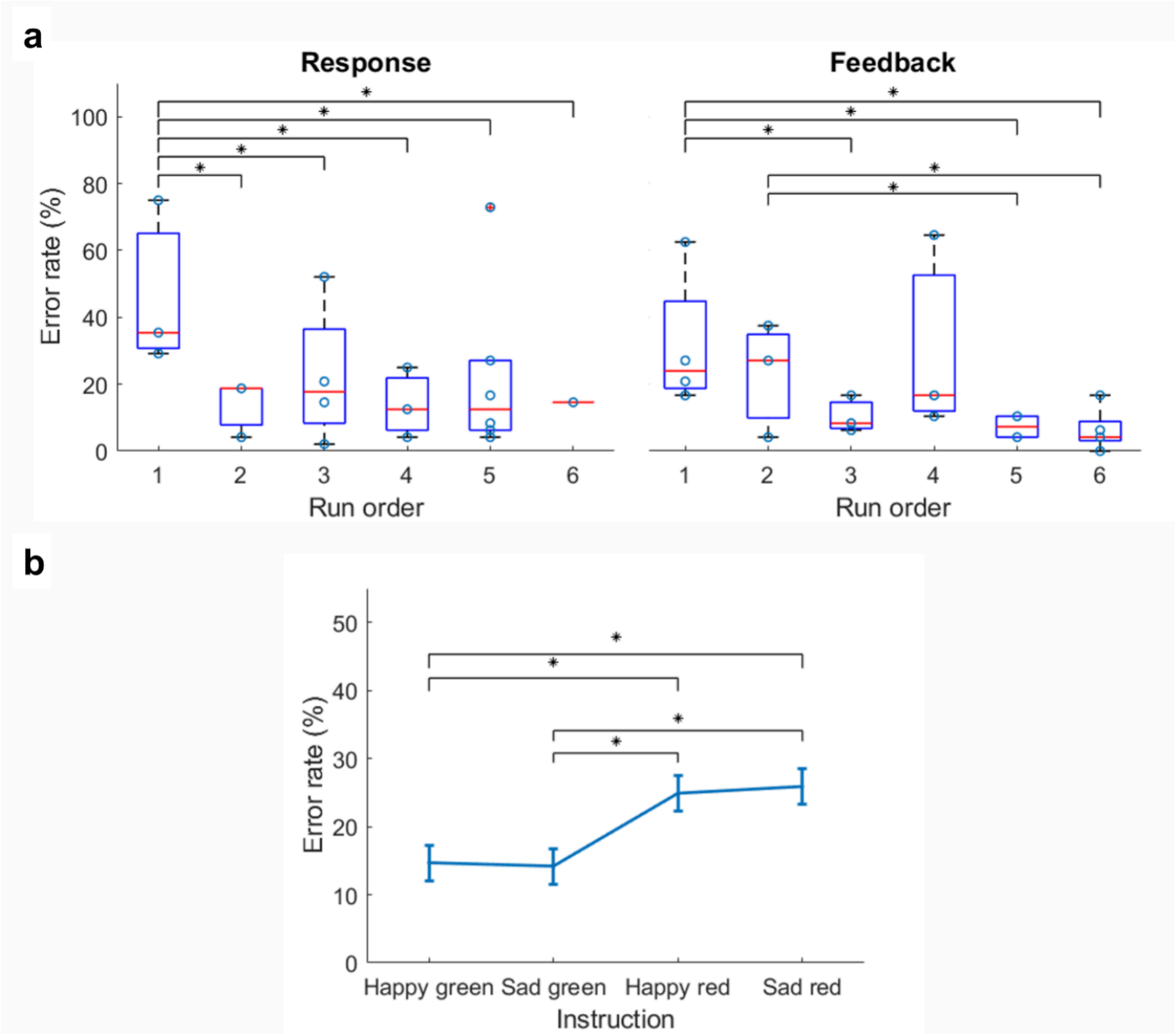


Figure 3

Behavioural results. (a) Scatter boxplots showing participants' error rate across experimental runs (1 to 6) for the response and feedback conditions. Due to the pseudo-randomized run order, the number of participants performing each condition at a given run position was not uniform. For example, only one participant completed the response condition in run 6, resulting in a single data point for that run. (b) Estimated marginal means of error rate for each instruction type (happy green, happy red, sad green, and sad red) during the response and feedback runs. Error rates were significantly influenced by the interaction between condition and run order/learning period, as well as by instruction type. These rates decreased with time and varied across instructions, reflecting distinct learning periods and difficulty levels. Significant differences in error rate ($p < 0.05$, Bonferroni-corrected) are signalled with an asterisk and error bars represent the standard error of the mean (SEM). See also Supplementary Table S1

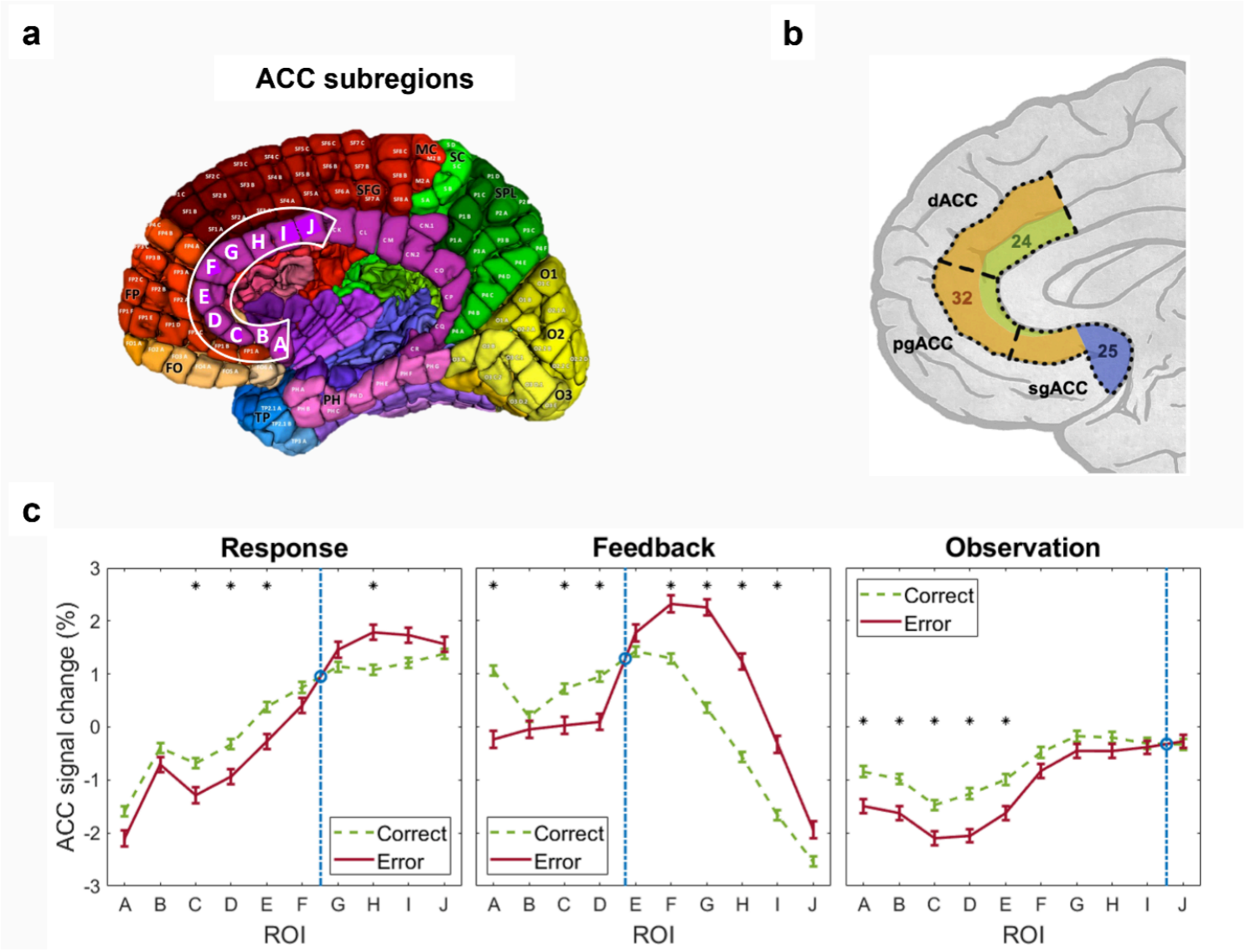


Figure 4

ACC response to errors depending on the condition, subregion, and performance. (a) The Yale high-resolution atlas (Mcgrath et al. 2022), used to define the ACC subregions (labelled A to J – from the most ventral to the most dorsal subregion). (b) Anatomical subdivisions of the ACC based on Alexander et al. (2021), illustrating the approximate distribution of Brodmann areas 24, 25, and 32 across the sgACC, pgACC, and dACC. From Alexander et al. (2021), licensed under CC BY 4.0. It should be noted that the anatomical boundaries and terminology used to define ACC subregions vary across studies and parcellation schemes. No single widely adopted atlas provides an explicit and consistent delineation of the dACC, pgACC, and sgACC. We therefore use these subdivisions as an anatomical framework for interpretation rather than as a formal parcellation of the Yale Brain Atlas parcels. (c) Estimated marginal means of percent signal change (PSC) betas for correct (green dashed line) and error events (red solid line) across ACC subregions for the response, feedback, and observation conditions. Error bars represent the SEM. Significant differences ($p < 0.05$, Bonferroni-corrected) between correct and error events are signalled with an asterisk. In all conditions, activity in the rostroventral subregions was diminished following errors compared to correct actions. In the response and feedback conditions, this

pattern reversed in the dorsal subregions, with greater activity following errors. In the observation condition, activity following correct and error events converges in the most dorsal part of the ACC. The reversal points — where correct and error lines intersect — are highlighted in blue. See also Supplementary Table S2

Supplementary Files

This is a list of supplementary files associated with this preprint. Click to download.

- SupplementaryInformation.docx